journal

J. Am. Ceram. Soc., 95 [11] 3657–3664 (2012)
DOI: 10.1111/j.1551-2916.2012.05390.x

Structural and Physical Property Studies of Amorphous Zn–In–Sn–O Thin Films

Diana E. Proffit,[‡,†] Qing Ma,[§] Donald B. Buchholz,[‡] Robert P. H. Chang,[‡] Michael J. Bedzyk,[‡] and Thomas O. Mason[‡]

[‡]Department of Materials Science and Engineering, Northwestern University, Evanston, Illinois 60208

[§]DND-CAT, Northwestern Synchrotron Research Center at Advanced Photon Source, Argonne, Illinois 60439

The structures in amorphous (*a*-) Zn, Sn co-doped In_2O_3 (ZITO) thin films grown by pulsed laser deposition on glass under varying oxygen pressure or with varying Sn:Zn ratios were determined using X-ray absorption spectroscopy and anomalous X-ray scattering. Typical structures around cations in *a*-ZITO films are described and compared with crystalline (*c*-) ZITO films. The results show that the Zn cations are four-fold coordinated with Zn–O bond lengths of 1.98 ± 0.02 Å, which is close to that in bulk ZnO. As a consequence, the second coordination shells around Zn contract. At longer distances away from Zn, the structure is commensurate with the averaged structure. The unit volume around In also contracts slightly compared to bulk In_2O_3, whereas the Sn–O bond length is similar to the one in bulk SnO_2. These unique structural characteristics may account for the films' superior thermal stability over amorphous Sn-doped In_2O_3, and suggest that Zn and Sn act as network-forming cations. Like in *c*-ZITO, coordination numbers (*N*) around Sn, In, and Zn follow the order $N_{Sn} > N_{In} > N_{Zn}$. Unlike in *c*-ZITO, where electrical properties change significantly with a slight variation in the Sn: Zn ratio, this variation does not markedly alter the electrical properties, or the local structures, of *a*-ZITO films. Dramatic changes in the electrical properties occur for films grown under various oxygen pressures, which point to oxygen "defects" as the source of charge carriers.

I. Introduction

Transparent conducting oxides (TCOs) combine high electrical conductivity with optical transparency in the visible region, making them essential in transparent electrode applications.[1–3] Their expanding use in photovoltaics, light emitting diodes, flat panel displays, and even thin film transistors requires an improved understanding of their processing-structure-property relationships to improve performance. In addition, the need for low temperature processing to enable deposition on plastics for flexible electronics is driving research in amorphous (*a*-) TCOs. Amorphous TCOs have electrical and optical properties similar to their crystalline counterparts,[4] but exhibit lower surface roughness, improved interfacial contacts, and better mechanical properties.[5–10]

Historically, the industry standard for high conductivity TCOs has been Sn-doped In_2O_3 (ITO).[11] Due to the volatile cost of indium, a search for lower indium content alternatives is ongoing.[4] One such alternative is the solid solution $In_{2-2x}Sn_xZn_xO_3$ ($x \leq 0.4$) (ZITO) in which In_2O_3 is codoped with equal amounts of Zn and Sn.[12,13] The high degree of codoping significantly reduces the indium content. This material retains the bixbyite structure of In_2O_3 and ITO, and so maintains similar properties.

A comprehensive study has been made of the processing-property relationships in amorphous $In_{2-2x}Sn_xZn_xO_3$ ($x \approx 0.3$) (ZITO30) thin films deposited via pulsed laser deposition (PLD).[14] An understanding of the local structures in *a*-ZITO films would complete the processing-structure-property relationship link. The local structure of crystalline (*c*-) ZITO30 thin films has been examined,[15] but the structure of *a*-ZITO films is not known.

The objective of this work was to determine the local structure of *a*-ZITO thin films grown by PLD using X-ray absorption spectroscopy (XAS) and anomalous X-ray scattering. Following a brief background of these techniques, a review of the local structures of In_2O_3, ITO, *c*-ZITO, and other *a*-TCOs is given as context for understanding and interpreting the structure-property relationships of *a*-ZITO films.

II. Background

X-ray absorption spectroscopy is a powerful tool for determining the local structures around specific absorbing atoms.[16] It is particularly useful for amorphous materials whose structures lack long-range periodicity. The X-ray absorption near-edge structure (XANES) contains information about chemical state and site symmetry. The X-ray absorption fine structure (EXAFS) contains information about interatomic distances, R_i, the root mean square statistical deviation of distances due to thermal motion and/or static disorder, σ_i^2, and coordination numbers, N_i. The EXAFS spectrum is analyzed via the equation

$$\chi(k) = \sum_i \frac{N_i(\theta)\ |f_i(k)|\ S_0^2}{kR_i^2} \sin\left[2R_ik + \phi(k) + \frac{4}{3}C_3k^3\right] \times e^{\frac{-2R_i}{\lambda(k)}} e^{-2\sigma_i^2k^2}$$

where S_0^2, the intrinsic loss factor, and $e^{-2Ri/\lambda(k)}$, the attenuation factor due to the electron mean free path, $\lambda(k)$, are determined using a suitable reference material, and where $e^{-2\sigma_i^2k^2}$ is the Debye–Waller factor. $|f_i(k)|$ and $\phi(k)$ are the backscattering amplitude and phase shift of traveling photoelectrons. Note that the angular dependence of N_i is negligible in amorphous materials.[16] The EXAFS third cumulant, C_3, can be used to account for the effect of an anharmonic potential on the measured interatomic distances.[16] In practice, this parameter (or any other additional parameter) is only included if the quality of the fit is significantly increased by its use, which in this case indicates an asymmetric distribution at that atomic site. A Fourier transform of $\chi(k)$

N. J. Dudney—contributing editor

Manuscript No. 31066. Received February 12, 2012; approved July 03, 2012.
†Author to whom correspondence should be addressed. e-mail: diana.proffit@gmail.com

produces the *pseudo*-radial distribution function (*p*-RDF) around the absorbing atom.

Due to the limited length of $\lambda(k)$, often only the first coordination shell structure is measured by EXAFS in amorphous materials. Also, the phase complication caused by disorder renders it difficult to reliably determine coordination numbers. The anomalous X-ray scattering technique has proven to be unique, as well as complementary, to the EXAFS technique.[17–19] It directly probes the electron density around a specific element and provides both short and medium range structural information without phase complication. For an X-ray scatterer (i.e., a given atomic species), the scattering intensity is proportional to f^2, where f is the scattering factor and is equal to $f_0 + f' + if''$. The f_0 term is the normal atomic form factor (also known as the Thomson scattering factor), the f'' term is associated with absorption, and the f' term is the resonance of f'', which is related optically by the Kramers–Kronig inversion. As a result, f varies strongly around the absorption edge of an atomic species. This variation provides enough contrast between the scattering intensities measured near the absorption edge and, normally, at one or a few hundred electron volts below the absorption edge that the difference of these two measurements allows one to obtain a differential structure factor (DSF). The Fourier transform of the DSF produces a differential pair distribution function (*d*-PDF) centered on the atom whose absorption edge is used. In this work, this technique is used to complement the XAS technique.

The parent compound of the ZITO solid solution is In_2O_3, which has the *bcc* bixbyite structure (space group *Ia*3, number 206).[20] Bixbyite is a fluorite-derivative structure with one quarter of the anions missing, resulting in a periodic structure with "structural vacancies" (oxygen interstitial positions). The unit cell has 80 atoms, 32 of which are indium cations. The cations are split between the *b*-sites (8 atoms, 25%) and the *d*-sites (24 atoms, 75%). All indium cations are surrounded by six oxygen atoms and two structural vacancy (interstitial) positions. At the *b*-site, the structural interstitial positions sit at body diagonal positions such that six oxygen atoms are equidistant at 2.18 Å. At the *d*-site, the structural interstitial positions sit at face diagonal positions such that two oxygen atoms sit at each of three distances (2.13, 2.19, 2.23 Å). The coordination numbers of the first three shells are $N_1 = N_2 = N_3 = 6$ and the lattice constant is 10.117 Å.

In Sn-doped In_2O_3, Sn substitutes on In sites and acts as an electron donor.[21–23] However, many of these donors form neutral associates with oxygen interstitials, $(2Sn_{In}^{\bullet}O_i'')^{\times}$, in so-called Frank–Köstlin (F–K) clusters. These donors must be activated by reducing the material to remove oxygen from the interstitial positions. F–K clusters indicate that the first shell around Sn in this structure can be easily over coordinated. The same clusters occur in *c*-ZITO.[24]

Previous studies show that Zn and Sn are substitutional dopants (on In sites) for both bulk *c*-ZITO ($In_{2-2x}Sn_xZn_xO_3$, $x = 0.1, 0.2, 0.3, 0.4$) [25] and thin film *c*-ZITO30.[15] However, due to the smaller ionic radii of Zn and Sn, they have smaller cation-oxygen bond lengths. In both bulk and film, the In –O bond length was 2.16 Å, which is very close to that of In_2O_3. In contrast, the Zn–O bond distance in bulk was 2.08 Å and in the thin film, ranged from 2.04–2.18 Å. In both materials, the disorder around Zn was high. In bulk, the Sn–O bond length was 2.08 Å and in the thin film there were two distances, at 2.08 and 2.25 Å. The disorder around Sn was similar to that around indium. In addition to these basic structures, a structural rearrangement was proposed in the thin film ZITO30 case, in which oxygen shifts from a site around Zn to a structural interstitial position around Sn. It also appears that in the thin film, Sn is likely over coordinated by oxygen when not compensated by Zn, forming F–K-like clusters.

The local structures of other amorphous materials, such as In_2O_3,[26] In–Zn–O (IZO),[27,28] In–Ga–Zn–O (IGZO),[29,30] and ZITO[31] have been investigated by EXAFS and X-ray scattering combined with computational methods such as molecular dynamics, reverse Monte Carlo, and density functional theory. The In-O bond length is fairly consistent across these materials at 2.11–2.14 Å, the only exception being one *a*-IGZO study[30] (the In–O bond length was 2.24–2.30 Å). In general, the bond length is consistently shorter than in the crystalline case and appears to be independent of the cation composition. The coordination number around indium lies in the range of 5–6. Rosen *et al.*[32] modeled various quasi-amorphous structures of In_2O_3 and ITO using molecular dynamics and saw that an increase in disorder resulted in a decrease in the average coordination number due to the appearance of 4- and 5-coordinated In and 3-coordinated oxygen. The Zn–O bond length in *a*-TCOs is also somewhat consistent at 1.95–1.97 Å, except for the same *a*-IGZO study[30] (the Zn–O bond length was split at 1.91 and 2.10–2.12 Å) and one *a*-IZO study[28] (the bond length was 2.02–2.03 Å). The Zn–O bond length is quite short versus the bond lengths in the crystalline counterparts, but matches well with the bond length in *c*-ZnO (1.96 Å). However, in ZnO, Zn is 4-coordinated. It should be noted that in most *a*-TCOs studied to date, with the two exceptions mentioned above (*a*-IGZO, *a*-IZO), Zn was found to be 4-coordinated. These studies provide a basis of comparison for the results of the present work.

III. Experimental Procedure

(1) Thin Film Preparation

Amorphous ZITO thin films were grown by pulsed laser deposition (PLD) on ~10 mm × 10 mm glass substrates at room temperature. A 248 nm KrF excimer-laser was operated at 2 Hz with 25-ns pulse duration and pulse energy of 200 mJ/pulse. The beam was focused to a 1 mm × 2 mm spot. To prevent local heating, the target was rotated at 5 rpm and the laser beam was rastered. The target-substrate separation was fixed at 10 cm. A dense, hot-pressed, ceramic ZITO target with a metallic composition of 70.3 at.% In, 13.4 at.% Sn and 16.3 at.% Zn was used. A series of three films were grown under varying deposition oxygen pressure (0.5, 7.5, and 15 mTorr) for measurement by XAS. Two more films were grown at 7.5 mTorr with the use of a second target (dense SnO_2) to slightly increase Sn concentration in the films. A computer controlled shuttle was used to alternate ablation between the ZITO and SnO_2 targets. Less than one monolayer of material was deposited in a typical ZITO-SnO_2 cycle to help insure a uniform distribution of Sn within the film. Last, an additional film was grown on a 10 mm × 25 mm glass substrate at 7.5 mTorr oxygen pressure to a larger thickness of 500 nm (as estimated from known growth rate and growth time) for the anomalous X-ray scattering study.

(2) Composition and Electrical Property Characterization

The metallic compositions of the ZITO target and films were measured using energy dispersive X-ray analysis (EDX) in a scanning electron microscope (Hitachi S4500; Tokyo, Japan). Multiple measurements of the ZITO target gave a compositional standard deviation of 1 at.%. Sheet resistance, carrier type, area carrier concentration, and carrier mobility of the films were measured via a Hall measurement system (Bio-Rad Microscience LTD HL5500) in the Van der Pauw configuration with a 0.320 Tesla field. The carrier density and resistivity were obtained by dividing the area carrier concentration and the sheet resistance by the film thickness, respectively. Film thicknesses were measured using a spectral reflectometer (Filmetrics F20; San Diego, CA) and were shown to range from 260–290 nm for thin films measured by EXAFS. X-ray diffraction (XRD) measurements (Rigaku ATX-G Workstation; Tokyo, Japan) were used to verify a lack of long-range order in the films.

(3) Synchrotron X-Ray Absorption Spectroscopy and Anomalous X-Ray Scattering

Synchrotron X-ray absorption and anomalous scattering measurements were made at the 5-BMD beamline of DND-CAT at the Advanced Photon Source (APS) of Argonne National Laboratory (Argonne, IL). The XAS data were collected by measuring the Zn-Kα, In-Kα, and Sn-Kα fluorescence emissions from *a*-ZITO thin films using a Canberra 13-element Ge solid state detector with an incident X-ray angle θ at ~45° with respect to the sample surface. A Si(111) double crystal monochromator was used. Two of the *a*-ZITO thin films were also measured at low temperatures in a modified Advanced Research System displex. Powder ZnO, In_2O_3, and SnO_2 were used as reference materials, for which the XAS data were collected in transmission mode. Reference powders were uniformly spread over Scotch tape and an appropriate number of tape layers were stacked to achieve statistically sound absorption. For the ZnO layers, caution was taken with regard to sample uniformity, since fewer layers were used due to low X-ray energies. The small-beam X-ray survey over the layered sample shows negligible variation in the transmitted intensities. Ion chambers (Oxford-Danfysik; Taastrup, Denmark) were used to monitor both the incident and transmitted X-ray intensities (I_0 and I_t), and were filled with gases in proportions of Ar: N_2=16:540 Torr for I_0 and 36:1360 Torr for I_t, respectively.

The XAS data were analyzed with the ATHENA software packages.[33] The S_0^2 values for Zn, In, and Sn were obtained using reference powders: $S_0^2 \approx 0.9$ for wurtzite ZnO and $S_0^2 \approx 1.0$ for rutile SnO_2 and bixbyite In_2O_3. These values all match well with those previously reported.[15,31] These S_0^2 values were then fixed in the data fitting. The structural model used to fit the *a*-ZITO films was a cluster of the bixbyite structure with a radius of 6 Å centered on the absorbing atom (In, Sn, or Zn). A Hanning window function was used in the Fourier transforms and data fitting. The stability of the fitting results was tested by varying the data range, which aided in error estimation as well. The results presented here were obtained using the EXAFS data in the *k* ranges from 3.268 to 11.091 $Å^{-1}$ for the In K-edge, 3.511 to 11.555 $Å^{-1}$ for the Sn K-edge, and 2.463 to 11.080 $Å^{-1}$ for the Zn K edge. Fittings were carried out in *R* space from 1.0 to 2.017 Å for the In K-edge and from 1.0 to 2.12 Å for both the Sn and Zn K-edges.

The Zn K-edge XANES calculations were carried out using the FDMNES code[34] in dipolar approximation. This code includes two approaches: the full-multiple-scattering (FMS) and the finite difference method (FDM). They differ in the cluster potential constructions. The FMS approach utilizes the spherical muffin-tin (MT) approximation, whereas the FDM approach utilizes a non-muffin-tin (NMT) numerical potential set on an equally spaced 3D-grid with a period of 0.25 Å. The FDM approach is sensitive to the geometrical details and can be carried out in a reasonable time for a small cluster, whereas the FMS computing is more rapid. The results from the FDM calculations are presented here. Electronic configurations of neutral Zn and In atoms were used in all the calculations; the Sn atoms were approximated by In ones. Except for the Fermi energy, which is determined self-consistently, the default parameters were used.

Anomalous X-ray scattering from the thicker *a*-ZITO film was measured around the Zn K-edge using a 4-element Si-drift detector (SII) mounted on the two theta (2θ) arm of a four-circle Huber diffractometer (Rimsting, Germany). The film was placed with the longer side along the X-ray beam. The measurements were carried out in glancing angle geometry with the X-ray incidence angle set near the critical angle so that no scattering from the substrate was seen. A vertically focused X-ray beam was employed for scattering experiments. The beam size was further defined by two pairs of Huber slits to height × width = 0.1 mm × 8 mm. The X-ray pulses were analyzed using the XMAP X-ray digital processing electronics (X-ray Instrument Associates; Hayward, CA). The peaking time was set at 1 μs, which is sufficiently fast for weak scattering from amorphous films. Therefore, no dead-time correction was needed. The four Si elements are squarely arranged, for which a double slit system was designed to separate the detectors into two pairs, each of which had a defined scattering angle (2θ). The angular offset between these two pairs of detectors were measured and applied to the collected data before merging them. For the measurements near the absorption edge, the Zn-Kα emissions were collected simultaneously in a separately defined range of interest (ROI). The ratio of Kβ/Kα was also measured using the photons 1 keV above the absorption edge, and was used to eliminate the Kβ content in the scattering intensities measured near the edge. For scattering measurements, the ROI was set large enough to include all the Compton scattering through the 2θ span (2–154°).

Anomalous X-ray scattering data were processed using the Igor-Pro commercial software and the Rad-Gtk+ package.[35] The scattering factors and Compton scattering factors were obtained from tabulated values.[36,37] The resonance terms f' and f'' were calculated from the XAS data measured on the film, and, for the Kramers–Kronig inversion, Sasaki's tabulated values were used to expand the data range to minimize the truncation effect.[38] The relevant X-ray energies were 9558.6 and 9658.6 eV (2.5 eV below the Zn K-edge) with respective calculated f' values of −4.27 and −8.91 and calculated f'' values of 0.49 and 1.18. The details regarding the data processing can be found in *Petkov*.[35]

IV. Results

(1) Electrical Properties of a-ZITO Films

As described above, films were grown under varying oxygen pressures (pO_2) and with varying Sn:Zn ratios at room temperature. Tables I and II summarize pertinent film growth conditions or metallic composition and the resulting electrical properties. Varying oxygen pressure during growth has a strong effect on the electrical properties, as seen in previous work[14] and in Table I: low pO_2 (0.5 mTorr) results in very low charge carrier concentration and mobility, midrange pO_2 (7.5 mTorr) maximizes both charge carrier concentration and mobility, and high pO_2 (15 mTorr) results in a low charge carrier concentration, but maintains high mobility. Conversely, varying the donor-to-acceptor ratio (Sn:Zn) has a negligible effect on the electrical properties, unlike in *c*-ZITO,[13] as seen in Table II. These properties will be discussed within the context of local structure below.

(2) Local Structures of a-ZITO

The XANES spectra for ZnO, the *c*-ZITO thin film,[15] and the 12:14 *a*-ZITO thin film are shown in Fig. 1. These spectra are representative of all *a*-ZITO films. The Zn K absorption edges of *a*-ZITO, *c*-ZITO, and ZnO are well aligned, indicating that Zn cations have a charge state of 2+. The same is true for In and Sn K-edge XANES, suggesting that In is 3+ and Sn is 4+. The In and Sn K-edge XANES spectra contain no discernible features that would highlight the

Table I. Electrical Properties of Films Deposited at Varying Oxygen Pressures with 12:14 Sn:Zn Ratio

Property	Units	p0.5	12:14	p15
Pressure	mTorr	0.5	7.5	15
σ	S/cm	7	1457	342
Hall mobility	$cm^2/V{\cdot}s$	1.4	49.5	53.0
n	$1/cm^3$	2.9×10^{19}	1.8×10^{20}	3.7×10^{19}

Table II. Electrical Properties of Films with Varying Sn:Zn Ratios Grown at 7.5 mTorr Oxygen Pressure

Property	Units	12:14	16:14	18:13
In	at.%	74.6	70.9	69.1
Sn		11.9	15.5	17.8
Zn		13.5	13.6	13.3
σ	S/cm	1457	1226	1431
Hall mobility	cm^2/V·s	49.5	48.4	46.7
n	$1/cm^3$	1.8×10^{20}	1.6×10^{20}	1.9×10^{20}

difference between *a*-ZITO and *c*-ZITO. This is due in part to the core-hole broadening in In and Sn and instrumental broadening [$\Delta E/E = 1.33 \times 10^{-4}$ for Si(111)], which overshadow broadening caused by disorder. The Zn K-edge XANES features of *a*-ZITO are markedly different, likely due to structural disorder. Modeling of this XANES spectrum will be presented later.

Figure 2 compares the phase-uncorrected *p*-RDFs of the 12:14 *a*-ZITO film (left) and the *c*-ZITO film[15] (right) for all three K-edges. The dashed lines are the EXAFS modeling results. In comparison to *c*-ZITO, only the first coordination shells were measured in *a*-ZITO due to disorder. Therefore, modeling was focused on the first coordination shells using the phases and amplitudes generated by the FEFF code based on a bixbyite In_2O_3 cluster centered at Zn, Sn, or In, respectively. The bond lengths, coordination numbers, and σ^2 values of all films except the p0.5 film are presented in Table III along with those of bulk oxides. The bond lengths are stable for all samples (including the p0.5 film), whereas the coordination numbers around a specific cation vary within ±10% (except the p0.5 film), i.e., largely within error, with no obvious trends related to composition and temperature. As a result, the *N* values in Table III have been consolidated to encompass all calculated values for the 12:14, 16:14, and 18:13 films prepared at 7.5 and 15 mTorr. The values listed include an average *N* value from the included films, the error bar for any given single film at that absorption edge, and the range in which the *N* values fell across the included films. Given the strong correlation between *N* and σ^2 [$x(k) \propto N \exp(-2\sigma^2k^2) \approx N(1-2\sigma^2k^2)$, $\sigma^2k^2 \ll 1$], a similar variation may occur in the σ^2 values. Although the *N* values are generally smaller than those found in *c*-ZITO,[15] the relation of $N_{Sn} > N_{In} > N_{Zn}$ is preserved for each sample, except for the p0.5 *a*-ZITO film, which will bve discussed later.

The bond lengths in *a*-ZITO are generally shorter than those in *c*-ZITO[15] although the error bars overlap for the In-O bond. However, the consistency of the In-O bond length (2.14 ± 0.02 Å) across samples and the agreement with values previously reported for amorphous In/O containing TCOs [26–29] suggest the bond length is slightly shorter than that in *c*-ZITO (2.17 ± 0.03 Å). The σ^2 value of the In–O bond is slightly larger in *a*-ZITO (0.0069–0.0092) than in *c*-ZITO (0.005–0.007). In addition, *N* around In is smaller in *a*-ZITO (5.0 ± 0.4) than in *c*-ZITO (~6), which is also consistent with previously reported values.[28,29] The Sn–O bond length (2.07 ± 0.03 Å) matches well with that in bulk SnO_2 (2.06 Å), both of which are similar to the shorter of the two bond lengths in *c*-ZITO (2.06 Å). Achieving an acceptable fit of the Sn K-edge data required the use of a C_3 parameter [16] due to significant peak asymmetry. The use of this parameter affects the calculated bond length, so these effects are included in the reported bond lengths and error bars. The σ^2 value around Sn is smaller than those around In and Zn in *a*-ZITO.

The structure around Zn in *a*-ZITO is different from that in *c*-ZITO.[15] The first coordination shell can be described satisfactorily by a single Gaussian distribution function centered at 1.98 ± 0.01 Å, which is significantly shorter than the bond length in *c*-ZITO (2.12 ± 0.06 Å),[15] but is very close to that in bulk ZnO (1.96 Å). Moreover, the coordination number around Zn (3.3 ± 0.2) appears to be significantly smaller than in *c*-ZITO (4.7 ± 0.6). These changes indicate a change to four-fold coordination around Zn cations in *a*-ZITO as opposed to the five-fold-coordinated Zn, on average, that sits on an octahedral site in *c*-ZITO.

Given the difficulties that EXAFS often presents in determining coordination numbers and the seemingly small coordination number around Zn obtained by EXAFS modeling, anomalous X-ray scattering was performed on the specially prepared (thicker) film similar in composition to the 12:14 film. Figure 3 compares the averaged PDF versus the *d*-PDF around a Zn atom. The Fourier transform was performed using scattering data up to $q(=4\pi\sin\theta/\lambda) = 9$ Å^{-1}. Because there are no phase effects in PDFs, atomic distances can be obtained directly from the peak positions. However, due to the limited *q* range, the uncertainty is large. The Zn–O bond length (1.9 ± 0.1 Å) is clearly shorter than the average metal (M)–O bond length in *a*-ZITO (2.08 ± 0.05 Å), thus supporting the EXAFS findings. In addition to the first coordination

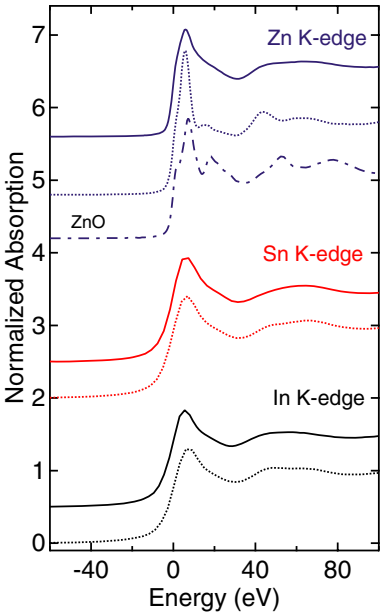

Fig. 1. XANES spectra of Sn:Zn = 12:14 *a*-ZITO thin film (solid lines), *c*-ZITO thin film (dotted lines),[15] and ZnO oxide (dot-dash line) for In K-edge (black), Sn K-edge (red), and Zn K-edge (blue). Data are shifted vertically for clarity.

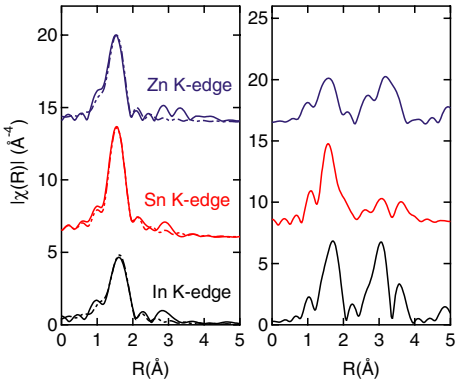

Fig. 2. Comparison of the In K-edge (black), Sn K-edge (red), and Zn K-edge (blue) *p*-RDFs of the Sn:Zn = 12:14 *a*-ZITO thin film (left) and *c*-ZITO thin film[15] (right). The dash-dot lines are the model fits of the *a*-ZITO data. Data have been shifted vertically for clarity.

Table III. Average Local Structures in All *a*-ZITO Films, Except p0.5, Compared to In_2O_3, SnO_2, and ZnO

	Bond length (Å)[†, ‡]		Coordination number[‡]		σ^2(Å^2) at 300 K	
Bonds	Bulk oxide[§]	*a*-ZITO	Bulk oxide	*a*-ZITO *N*(SSD, range)	Bulk oxide	*a-ZITO*
In–O	2.18	2.14 (±0.02)	6	5.0 (±0.4, −0.5 to 0.5)	0.0059	0.0069–0.0092
Sn–O	2.06	2.07 (±0.03)	6	5.9 (±0.3, −0.4 to 0.6)	0.0030	0.0057–0.0067
Zn–O	1.96	1.98 (±0.01)	4	3.3 (±0.2, −0.2 to 0.3)	0.0043	0.0065–0.0081

[†]Error bars for distance ranges include C_3 effects.
[‡]Bond lengths and coordination numbers are averaged over compositions and temperatures.
[§]Bulk oxides: In_2O_3, SnO_2, and ZnO.

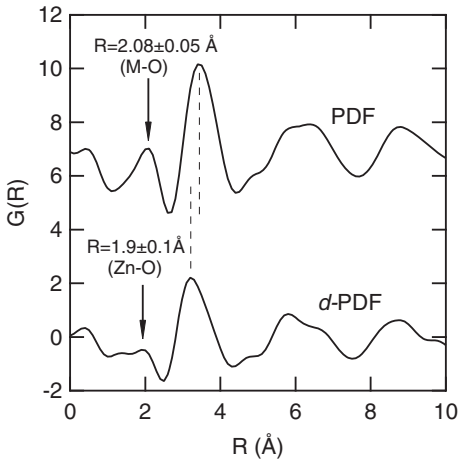

Fig. 3. Top: The pair distribution function (PDF) of the average *a*-ZITO structure. Bottom: The difference pair distribution function (*d*-PDF) of the structure around Zn in *a*-ZITO.

shell, the higher coordination shells are clearly seen. The second shell distance around Zn (Zn–M or –O) is also shorter than the averaged one. At longer distances away from Zn, the structure becomes more commensurate with the averaged structure, which indicates no phase segregation of ZnO in the *a*-ZITO film. The radial distribution function (RDF) can be obtained from $G(R)$ using $4\pi R\rho = 4\pi R\rho_0 + RG(R)$, where ρ is the density and ρ_0 is the average density. The peak areas in the RDF measure the electron densities and, thus, the coordination numbers. For a multi-element system, the integrated area of a RDF peak is approximately equal to the weighted sum of the coordination numbers.[19] Using the scattering factors at $q = 0$, such a weighted sum in *a*-ZITO is estimated to be 9 if all cations are 6-coordinated (by oxygen anions) and all oxygen anions are 4-coordinated (by all cations), like in In_2O_3. If Zn is 4-coordinated, the weighted sum is 8. In contrast, the weighted sum of the *d*-RDF is 7 if Zn is 4-coordinated or 10 if it is 6-coordinated. Therefore, the smaller first peak in the *d*-PDF compared to the PDF suggests $N < 6$ around Zn, which qualitatively supports the EXAFS results. More elaborate data simulation is necessary to quantify the Zn K-edge data.[18,19]

EXAFS and anomalous scattering revealed the local structures in *a*-ZITO, but the local geometry, in particular around Zn, is not clear. Since XANES is sensitive to electronic structure and local geometry, detailed analysis of the Zn K-edge XANES of the *a*-ZITO film provides a better understanding of the structure. Figure 4 compares the results of the XANES calculations using the FDM approach (A, B, C) with the experimental XANES spectrum (dotted line) of 12:14 *a*-ZITO. Since the XAS data are dominated by the first coordination shell in *a*-ZITO, the local geometries around Zn used in the calculation are generated from a simplified (disordered) *d*-site in bixbyite, as shown below. The oxygen atoms are labeled according to bond length such that

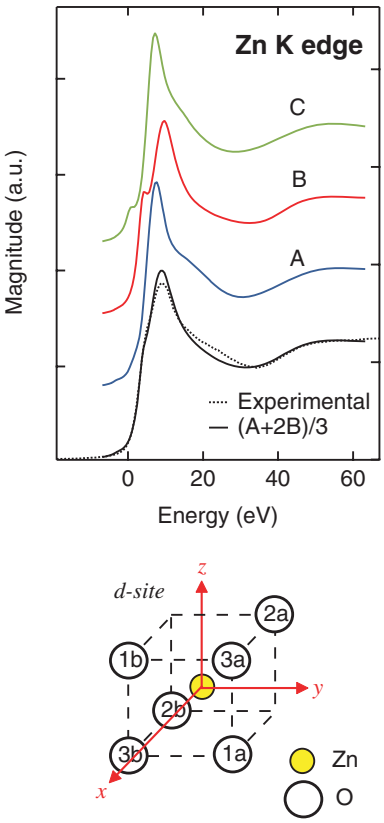

Fig. 4. Top: First shell FDM calculations (A, B, C) for different local geometries around Zn in *a*-ZITO using the simplified (disordered) *d*-site in bixbyite (bottom) compared to the experimental XANES measurement (dotted line). Bottom: The oxygen atoms are labeled according to bond length such that Zn–$O_{1a,1b}$ = 2.19 Å, Zn–$O_{2a,2b}$ = 2.12 Å, and Zn–$O_{3a,3b}$ = 2.21 Å. The calculation A removed O_{3a} and O_{3b} to form a tetrahedral local structure, the calculation B removed O_{1a} and O_{1b} to form a planar structure, and the calculation C removed O_{2a} and O_{2b} to form a pyramidal structure.

Zn–$O_{1a,1b}$ = 2.19 Å, Zn–$O_{2a,2b}$ = 2.12 Å, and Zn–$O_{3a,3b}$ = 2.21 Å. The calculation (A) removed O_{3a} and O_{3b} to form a tetrahedral local structure, the calculation (B) removed O_{1a} and O_{1b} to form a planar structure, and the calculation (C) removed O_{2a} and O_{2b} to form a pyramidal structure. In each case, the bond lengths were contracted by 5% to better match the feature positions. This is consistent with the shorter bond lengths measured by EXAFS. The removal of two oxygen atoms was also necessary to obtain a reasonable match to the magnitude of the features, which again is consistent with the small coordination number determined by EXAFS. Comparing the calculated versus measured XANES spectra, it appears that a combination of planar and tetrahedral local geometries would best match the experimental data, although other geometries could exist.

Although the local structures presented in Table III represent all but one of the films, the thermal responses of the local structures do show an interesting compositional dependence, as revealed by temperature–dependent XAS measurements. Figure 5 overlays, for each absorption edge, the first shell EXAFS oscillations of the Sn:Zn = 12:14 and 16:14 *a*-ZITO films obtained by back Fourier transforms of the first shell peaks (with R = 1–2 Å) at all three temperatures (78, 165, and 300 K). The Zn environment in the Zn-rich film (12:14) changes only slightly with temperature, although changes are quite noticeable in the In and Sn environments. The opposite is true in the Sn-rich film (16:14). The FEFF fits of these data indicate that these structural changes can be accounted for mostly by changes in the Debye–Waller factor $e^{-2\sigma_i^2 k^2}$, indicating their thermal nature. Figure 6 plots σ^2/N vs T for the 12:14 and 16:14 *a*-ZITO films. Given the high correlation between N and σ^2, σ^2/N should minimize the effect of this correlation on the analysis. The error bars in Fig. 6 were obtained as follows

$$\pm\frac{\overline{\sigma^2}+\Delta\sigma^2_{\mathrm{SSD}}}{\overline{N}-\Delta N_{\mathrm{SSD}}},$$

where SSD is the sample standard deviation $[=\sqrt{\sum_1^n((x_j-\bar{x})/(n-1))}]$. These results show again that despite essentially indistinguishable (by EXAFS) local structures across compositions, compositional changes do result in different thermal responses. Unlike in crystalline materials where atoms act *coherently*, the rigidity of the local structure in an amorphous material could vary depending on the geometrical details of the overall structure. However, the overall structural rigidity may be reflected in the thermal responses of the In–O bonds since In is the majority cation in the films.

As mentioned above, the p0.5 *a*-ZITO film has a slightly different structure than the other films, specifically in its coordination number around Sn. N is 4.1 ± 0.3 as compared to 5.9 ± 0.3 in the other *a*-ZITO films. This coordination number matches more closely to SnO (and the presence of Sn^{2+}) than SnO_2, which aligns well with the relatively reducing deposition conditions of this film (as compared to the others). The other structural parameters fall within the ranges noted in Table III.

V. Discussion

The XAS and anomalous X-ray scattering results reveal details about the local structures of *a*-ZITO, and how they differ from those in *c*-ZITO. In *a*-ZITO, the In–O bond length is likely slightly smaller than that in *c*-ZITO, whereas the Sn–O bond length is similar to the shorter length in *c*-ZITO. N_{In} is significantly smaller than N_{Sn} (see Table III). Given the similarity in the *a*-ZITO and *c*-ZITO XANES around In and Sn (despite broadening), we speculate that their first shell structures likely maintain a similar geometry.

The first shell structure around Zn has a bond length of 1.98 Å. This indicates a significant volume contraction of ~25% compared to a cubic site in the bixbyite structure, which results in a lower coordination around Zn. Also as a consequence, the second shell structure contracts toward Zn, as found using anomalous X-ray scattering. However, the structure at longer distances becomes commensurate with the average structure. The smaller, four-fold coordinated Zn may be important in stabilizing the structural framework of *a*-ZITO. These films have a much higher crystallization temperature (T_c - from our recent work, 300°C–345°C) than that of *a*-In_2O_3 (165°C–210°C)[39] and *a*-ITO (185°C–230°C).[40] Both the medium range order and higher T_c of *a*-ZITO are consistent with a homogeneous amorphous phase in the films.

Linking the local structures to the electrical properties in *a*-ZITO is a significant challenge. In *c*-ZITO, it has been proposed that Sn donors compensated by Zn acceptors participate in a structural rearrangement in which Sn gains an oxygen atom at the expense of a Zn cation.[15] This rearrangement maintains charge balance and stoichiometry, while satisfying the preference of Zn to have a lower coordination. It is also consistent with the tendency of Sn donors to stabilize extra oxygen, as seen in the F-K clusters formed by excess Sn donors.[15,24] As a result, the coordination number trend in *c*-ZITO is $N_{\mathrm{Sn}} > N_{\mathrm{In}} > N_{\mathrm{Zn}}$.

Interestingly, despite generally smaller N values, this trend persists in *a*-ZITO. Sn tends to be over coordinated, whereas

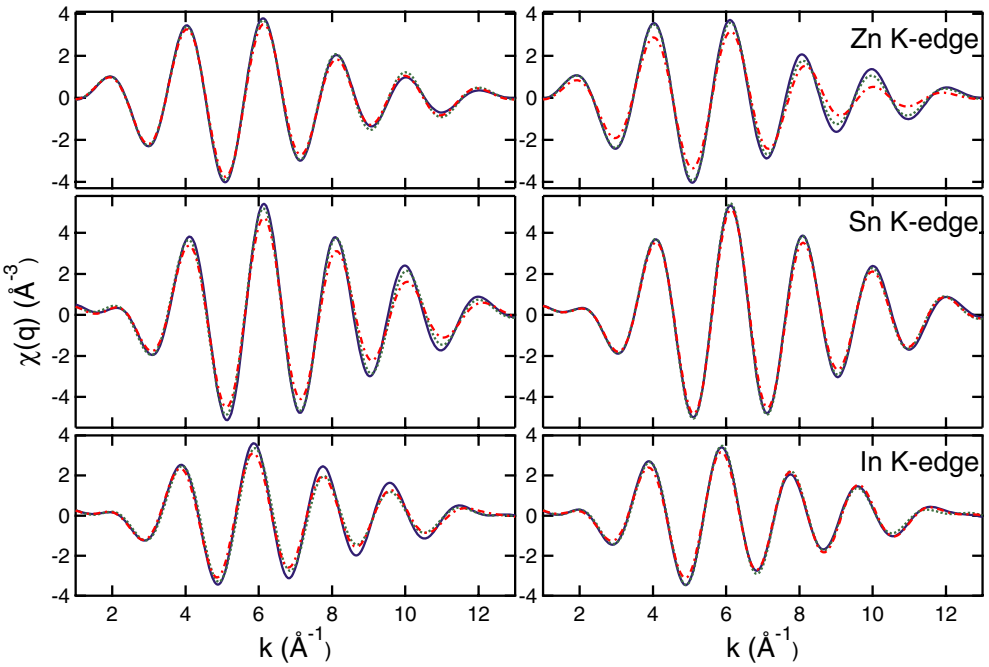

Fig. 5. Overlays of the first shell back Fourier transforms of the In, Sn, and Zn K-edges for the Sn:Zn = 12:14 (left) and 16:14 (right) *a*-ZITO films measured at 78 K (blue solid line), 165 K (green dotted line), and 300 K (red dash-dot line).

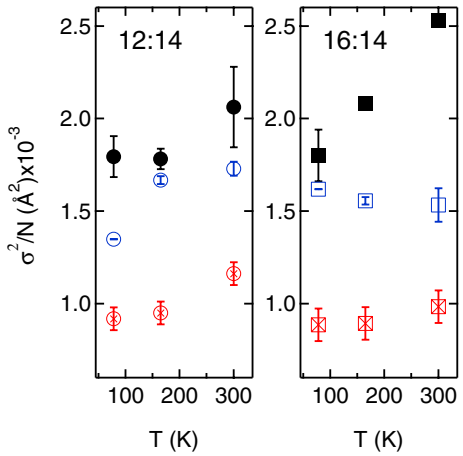

Fig. 6. σ^2/N vs T for the *a*-ZITO films with Sn:Zn = 12:14 (circles - left) and 16:14 (squares - right) deposited at 7.5 mTorr. Solid black markers indicate Zn–O bonds, open blue markers indicate In–O bonds, and crossed red markers indicate Sn–O bonds.

Zn tends to be under coordinated when compared to In. However, in *a*-ZITO, changes in the Sn:Zn (donor:acceptor) ratio do not result in significant changes in the electrical properties (Table II). This suggests that Sn and Zn function as network-forming cations (along with In) rather than as "dopants" (donor/acceptor).

In contrast, electrical properties change significantly with changes in oxygen pressure during deposition. However, EXAFS measurements show no significant difference between the local structures of the films deposited at 7.5 and 15 mTorr, despite the large difference in their carrier concentrations (see Table I). This is not surprising, since the oxygen "defect" donor (e.g., "vacancies") population would be on the order of the carrier concentration (10^{19}–10^{20} cm^{-3}), which is relatively small compared to the overall oxygen concentration in *a*-ZITO (~10^{22}/cm^3). The results in Tables I and II suggest that oxygen "defects" play a dominant role in charge carrier creation.

The only *a*-ZITO film with a unique local structure compared to the others was that deposited at the most reducing conditions (0.5 mTorr). Although the bond lengths, σ^2 values, and coordination numbers around In and Zn match those listed in Table III, the coordination number around Sn dropped from 5.9 ± 0.3 to 4.1 ± 0.3. This local structure change is accompanied by large drops in mobility and charge carrier concentration (Table I), as well as a drop in optical transmittance.[14] These factors suggest the presence of Sn^{2+} cations. Thus, under highly reducing conditions, Sn^{2+} will form leading to the detriment of the electrical and optical properties, which should be avoided.

VI. Conclusions

The local structures in *a*-ZITO thin films made by PLD were investigated using EXAFS and anomalous X-ray scattering and compared to those in *c*-ZITO thin films. The bond lengths and coordination numbers around In and Sn are slightly smaller than those in *c*-ZITO, which in the case of In is consistent with other studies reported in the literature. However, the structure around Zn is unique. In *a*-ZITO, the Zn-O bond length is 1.98 Å and the four-fold first shell coordination environment consists of a mix of tetrahedral, planar and other disordered geometries. As a result, the second coordination shell contracts toward Zn. Despite these differences in local structure, the structural framework in *a*-ZITO does not depart drastically from that in *c*-ZITO. In fact, coordination numbers (N) around Sn, In, and Zn follow the same order as in *c*-ZITO, $N_{Sn} > N_{In} > N_{Zn}$, but are generally smaller. However, the unique structure around Zn may account for the increased crystallization temperature of *a*-ZITO compared to *a*-In_2O_3 and *a*-ITO. Also, unlike in *c*-ZITO, variations in the Sn:Zn ratio do not markedly change the electrical properties of *a*-ZITO. This suggests that Zn and Sn can be viewed as network-forming cations in the overall amorphous structure. On the other hand, variations in oxygen pressure during deposition dramatically change the electrical properties of *a*-ZITO, pointing to oxygen "defects" as the dominant donor species in *a*-ZITO.

Acknowledgments

This work is supported in part by the NSF MRSEC program at Northwestern University under grant no. DMR-1121262 (DBB, RPHC, MJB, TOM) and in part by the U.S. Department of Energy, Office of Basic Energy Sciences as part of an Energy Frontier Research Center (DOE, grant no. DE-SC0001059, DEP, RPHC, TOM). DEP acknowledges support of an NSF Graduate Research Fellowship. DND-CAT is supported by the E.I. DuPont de Nemours & Co., The Dow Chemical Co., the NSF via grant no. DMR-9304725 (MJB, QM) and the State of Illinois via Grant IBHE HECA NWU 96. The APS is supported by the DOE via Contract no. DE-AC02-06CH11357. The authors acknowledge helpful discussions with C. A. Hoel and K. R. Poeppelmeier.

References

[1]E. Fortunato, D. Ginley, H. Hosono, and D. C. Paine, "Transparent Conducting Oxides for Photovoltaics," *MRS Bull.*, **32** [3] 242–7 (2007).
[2]J. F. Wager, D. A. Keszler, and R. E. Presley, *Transparent Electronics*. Springer, New York, 2008.
[3]D. S. Ginley, H. Hosono, and D. C. Paine, *Handbook of Transparent Conductors*. Springer, New York, 2010.
[4]C. A. Hoel, T. O. Mason, J. F. Gaillard, and K. R. Poeppelmeier, "Transparent Conducting Oxides in the ZnO-In_2O_3-SnO_2 System," *Chem. Mater.*, **22** [12] 3569–679 (2010).
[5]T. Kamiya and H. Hosono, "Material Characteristics and Applications of Transparent Amorphous Oxide Semiconductors," *NPG Asia Mater.*, **2**, 15–22 (2010).
[6]J. Liu, D. B. Buchholz, R. P. H. Chang, A. Facchetti, and T. J. Marks, "High-Performance Flexible Transparent Thin-Film Transistors Using a Hybrid Gate Dielectric and Amorphous Zinc Indium Tin Oxide Channel," *Adv. Mater.*, **22** [21] 2333–7 (2010).
[7]M. P. Taylor, D. W. Readey, M. F. A. M. Van-Hest, C. W. Teplin, J. L. Alleman, M. S. Dabney, L. M. Gedvilas, B. M. Keyes, B. To, J. D. Perkins, and D. S. Ginley, "The Remarkable Thermal Stability of Amorphous In-Zn-O Transparent Conductors," *Adv. Funct. Mater.*, **18** [20] 3169–78 (2008).
[8]J. A. Jeong, H. K. Kim, and S. I. Na, "Low Resistance and High Transparent Amorphous IZTO Electrode Cosputtered by Linear Facing Target Sputtering for Organic Photovoltaics," *Electrochem. Solid-State Lett.*, **12** [9] J80–2 (2009).
[9]G. S. Heo, Y. Matsumoto, I. G. Gim, J. W. Park, K. Y. Kim, and T. W. Kim, "Fabrication of Cosputtered Zn-In-Sn-O Films and Their Applications to Organic Light-Emitting Diodes," *Solid State Commun.*, **149** [41–42] 1731–4 (2009).
[10]G. S. Heo, Y. Matsumoto, I. G. Gim, H. K. Lee, J. W. Park, and T. W. Kim, "Transparent Conducting Amorphous Zn-In-Sn-O Anode for Flexible Organic Light-Emitting Diodes," *Solid State Commun.*, **150** [3–4] 223–5 (2010).
[11]D. S. Ginley and C. Bright, "Transparent Conducting Oxides," *MRS Bull.*, **25** [8] 15–8 (2000).
[12]G. B. Palmer, K. R. Poeppelmeier, and T. O. Mason, "Conductivity and Transparency of ZnO/SnO_2-Cosubstituted In_2O_3," *Chem. Mater.*, **9** [12] 3121–6 (1997).
[13]S. P. Harvey, T. O. Mason, D. B. Buchholz, R. P. H. Chang, C. Körber, and A. Klein, "Carrier Generation and Inherent Off-Stoichiometry in Zn,Sn Co-Doped Indium Oxide (ZITO) Bulk and Thin Film Specimens," *J. Am. Ceram. Soc.*, **91** [2] 467–72 (2008).
[14]D. B. Buchholz, J. Liu, T. J. Marks, M. Zhang, and R. P. H. Chang, "Control and Characterization of the Structural, Electrical, and Optical Properties of Amorphous Zinc-Indium-Tin Oxide Thin Films," *ACS Appl. Mater. Interfaces*, **1** [10] 2147–53 (2009).
[15]D. E. Proffit, D. B. Buchholz, R. P. H. Chang, M. J. Bedzyk, T. O. Mason, and Q. Ma, "X-Ray Absorption Spectroscopy Study of the Local Structures of Crystalline Zn-In-Sn Oxide Thin Films," *J. Appl. Phys.*, **106** [11] 113524, 6pp (2009).
[16]J. J. Rehr and R. C. Albers, "Theoretical Approaches to X-Ray Absorption Fine Structure," *Rev. Mod. Phys.*, **72** [3] 621–54 (2000).
[17]P. H. Fuoss, P. Eisenberger, W. K. Warburton, and A. Bienenstock, "Application of Differential Anomalous X-Ray-Scattering to Structural Studies of Amorphous Materials," *Phys. Rev. Lett.*, **46** [23] 1537–40 (1981).
[18]Q. Ma, D. Raoux, and S. Bénazeth, "Local-Structure of As_XTe_{100-x} Glasses Studied by Differential X-Ray Anomalous Scattering and X-Ray Absorption Spectroscopy," *Phys. Rev. B*, **48** [22] 16332–46 (1993).
[19]Q. Ma, W. Zhou, D. E. Sayers, and M. Paesler, "Photoinduced Structural Changes in Amorphous As_2S_3 as Measured by Differential Anomalous X-Ray Scattering," *Phys. Rev. B*, **52** [14] 10025–34 (1995).

[20]M. Marezio, "Refinement of the Crystal Structure of In_2O_3 at Two Wavelengths," *Acta Cryst*., **20**, 723–8 (1966).
[21]G. B. Gonzalez, T. O. Mason, J. P. Quintana, O. Warschkow, D. E. Ellis, J. H. Hwang, J. P. Hodges, and J. D. Jorgensen, "Defect Structure Studies of Bulk and Nano-Indium-Tin Oxide," *J. Appl. Phys.*, **96** [7] 3912–20 (2004).
[22]G. Frank and H. Köstlin, "Electrical Properties and Defect Model of Tin-Doped Indium Oxide Layers," *Appl. Phys. A*, **27** [4] 197–206 (1982).
[23]S. P. Harvey, T. O. Mason, Y. Gassenbauer, R. Schafranek, and A. Klein, "Surface Versus Bulk Electronic/Defect Structures of Transparent Conducting Oxides: I. Indium Oxide and ITO," *J. Phys. D: Appl. Phys*., **39** [18] 3959–68 (2006).
[24]S. P. Harvey, T. O. Mason, C. Körber, and A. Klein, "Bulk Defect Chemistry and Surface Electronic Behavior of Zn, Sn Codoped In_2O_3 Transparent Conducting Oxides," *Phys. Chem. Chem. Phys*., **11** [17] 3099–104 (2009).
[25]C. A. Hoel, J. F. Gaillard, and K. R. Poeppelmeier, "Probing the Local Structure of Crystalline ZITO: $In_{2-2x}Sn_xZn_xO_3$ ($x \leq 0.4$)," *J. Solid State Chem*., **183** [9] 761–8 (2010).
[26]F. Utsuno, H. Inoue, I. Yasui, Y. Shimane, S. Tomai, S. Matsuzaki, K. Inoue, I. Hirosawa, M. Sato, and T. Honma, "Structural Study of Amorphous In_2O_3 Film by Grazing Incidence X-Ray Scattering (GIXS) with Synchrotron Radiation," *Thin Solid Films*, **496** [1] 95–8 (2006).
[27]F. Utsuno, H. Inoue, Y. Shimane, T. Shibuya, K. Yano, K. Inoue, I. Hirosawa, M. Sato, and T. Honma, "A Structural Study of Amorphous In_2O_3-ZnO Films by Grazing Incidence X-Ray Scattering (GIXS) with Synchrotron Radiation," *Thin Solid Films*, **516** [17] 5818–21 (2008).
[28]T. Eguchi, H. Inoue, A. Masuno, K. Kita, and F. Utsuno, "Oxygen Close-Packed Structure in Amorphous Indium Zinc Oxide Thin Films," *Inorg. Chem*., **49** [18] 8298–304 (2010).
[29]K. Nomura, T. Kamiya, H. Ohto, T. Uruga, M. Hirano, and H. Hosono, "Local Coordination Structure and Electronic Structure of the Large Electron Mobility Amorphous Oxide Semiconductor In-Ga-Zn-O: Experiment and *Ab Initio* Calculations," *Phys. Rev. B*, **75** [3] 035212, 5pp (2007).
[30]D. Y. Cho, J. Song, K. D. Na, C. S. Hwang, J. H. Jeong, J. K. Jeong, and Y. G. Mo, "Local Structure and Conduction Mechanism in Amorphous In-Ga-Zn-O Films," *Appl. Phys. Lett*., **94**, 112112, 3pp (2009).
[31]C. A. Hoel, S. Xie, C. Benmore, C. D. Mailliakas, J. F. Gaillard, and K. R. Poeppelmeier, "Evidence for Tetrahedral Zinc in Amorphous $In_{2-2x}Zn_xSn_xO_3$ (*a*-ZITO)," *Z. Anorg. Allg. Chem*., **637** [7–8] 885–94 (2011).
[32]J. Rosen and O. Warschkow, "Electronic Structure of Amorphous Indium Oxide Transparent Conductors," *Phys. Rev. B*, **80** [11] 115215, 10pp (2009).
[33]B. Ravel and M. Newville, "ATHENA, ARTEMIS, HEPHAESTUS: Data Analysis for X-Ray Absorption Spectroscopy Using IFEFFIT," *J. Synchrotron Radiat*., **12**, 537–41 (2005).
[34]Y. Joly, "X-Ray Absorption Near-Edge Structure Calculations Beyond the Muffin-Tin Approximation," *Phys. Rev. B*, **63** [12] 125120, 10pp (2001).
[35]V. Petkov, "RAD, a Program for Analysis of X-Ray Diffraction Data From Amorphous Materials for Personal Computers," *J. Appl. Crystallogr*., **22**, 387–9 (1989).
[36]D. Waasmaier and A. Kirfel, "New Analytical Scattering-Factor Functions for Free Atoms and Ions," *Acta Cryst. A*, **51**, 416–31 (1995).
[37]N. G. Alexandropoulos, M. J. Cooper, P. Suortti, and B. T. M. Willis, "Correction of Systematic Errors"; pp. 653–65 in *International Tables for Crystallography* Vol. C, Chapter 7.4, John Wiley & Sons, Hoboken, NJ, 2006.
[38]S. Sasaki, KEK Report 83-22, National Laboratory for High Energy Physics, Tsukuba, Japan, 1983.
[39]F. O. Adurodija, L. Semple, and R. Brüning, "Real-Time *In Situ* Crystallization and Electrical Properties of Pulsed Laser Deposited Indium Oxide Thin Films," *Thin Solid Films*, **492** [1–2] 153–7 (2005).
[40]F. O. Adurodija, L. Semple, and R. Brüning, "Crystallization Process and Electro-Optical Properties of In_2O_3 and ITO Thin Films," *J. Mater. Sci*., **41** [21] 7096–102 (2006). □